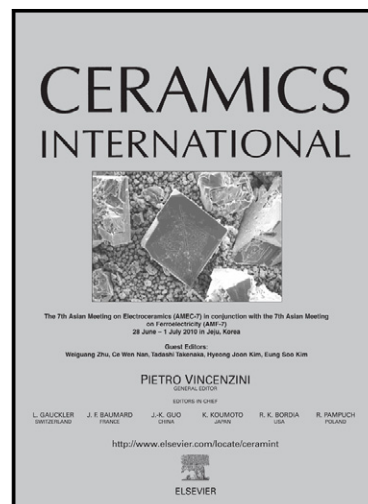# Author's Accepted Manuscript

Changes on structural and magnetic properties of maghemite nanoparticles during their coverage with MCM-41

Nicolás A. Fellenz, Ignacio O. Pérez De Berti, Analía L. Soldati, Silvana J. Stewart, Sergio G. Marchetti, José F. Bengoa

Cite this article as: Nicolás A. Fellenz, Ignacio O. Pérez De Berti, Analía L. Soldati, Silvana J. Stewart, Sergio G. Marchetti, José F. Bengoa, Changes on structural and magnetic properties of maghemite nanoparticles during their coverage with MCM-41, *Ceramics International,* http://dx.doi.org/10.1016/j.ceramint.2015.08.016

This is a PDF file of an unedited manuscript that has been accepted for publication. As a service to our customers we are providing this early version of the manuscript. The manuscript will undergo copyediting, typesetting, and review of the resulting galley proof before it is published in its final citable form. Please note that during the production process errors may be discovered which could affect the content, and all legal disclaimers that apply to the journal pertain.

Changes on structural and magnetic properties of maghemite nanoparticles during their coverage with MCM-41

Nicolás A. Fellenz[1], Ignacio O. Pérez De Berti[2], Analía L. Soldati[3], Silvana J. Stewart[4], Sergio G. Marchetti[2], José F. Bengoa[2*]

[1]Universidad Nacional de Rio Negro, CONICET, Belgrano 526, 8500, Viedma, Rio Negro, Argentina.

[2]Departamento de Química, Facultad de Ciencias Exactas, Universidad Nacional de La Plata, CONICET, CINDECA, CICPBA, 47 No 257, 1900 La Plata, Argentina.

[3]Grupo de Caracterización de Materiales, Centro Atómico Bariloche, CONICET, Av. Bustillo 9500, San Carlos de Bariloche, Río Negro, Argentina.

[4]IFLP-CCT-La Plata-CONICET and Departamento de Física, Facultad de Ciencias Exactas, C. C. 67, Universidad Nacional de La Plata, 1900 La Plata, Argentina

*corresponding autor.

Email : bengoajf@quimica.unlp.edu.ar

phone: +54-221-4210711

calle 47 No 257, (1900) La Plata, Argentina.

Abstract.

This work reports a simple synthesis of a mesoporous ordered silica structure (MCM-41) grown up around pre-synthesized maghemite nanoparticles. A composite with magnetic response and high specific surface area was obtained adding maghemite nanoparticles coated with oleic acid in the synthesis gel of MCM-41 and finally calcining in air. Different characterizations techniques such as magnetic measurements, Mössbauer spectroscopy at 25 and -260 ºC and transmission electron microscopy were used to study the magnetic and structural changes of the initial maghemite nanoparticles produced during its coverage with the mesoporous silica structure. The presence of the mesoporous structure inhibits the expected transformation from maghemite to hematite when the system was calcined in air at 510 ºC. It was established that a sintering of the nanoparticles during the calcination step occurs, leading to a magnetization saturation value similar to that of the bulk compound. In order to evaluate the capability as adsorbent, the magnetic composite was subjected to a surface amino-functionalization and then tested for Cr(VI) and Cu(II) adsorption from water.

1. Introduction

The potential applications of iron oxide magnetic nanoparticles (MNPs) in different fields such as pollutants adsorption from aqueous matrix, biomolecules separation, drug delivery, magnetic hyperthermia, enzymes immobilization, microalgae harvesting, etc. [1-7] have produced great efforts to reach a greater knowledge in basic and applied fields. All applications of these MNPs require a good dispersion in aqueous medium, chemical stability in the environment where it will be used and high values of specific

surface area (S_g) (the last conditions is not necessary in magnetic hyperthermia applications). However, if "naked" nanoparticles are used, the presence of magnetic interactions, especially dipolar interactions, produces agglomeration, clustering and subsequent precipitation [8]. On the other hand, in this condition, the specific surface area values are between 30 and 200 $m^2.g^{-1}$ [1, 9, 10] and, in order to use these systems in adsorption or separation processes, these areas are insufficient. The coverage of MNPs with different polymer networks has been used to solve these problems [9, 11-13]. This strategy reduces the formation of clusters and increases the S_g of the resulting composite. When SiO_2 compounds are used to cover the MNPs, the silanols groups present in their surface can be covalently modified with various functional groups. This increases the specificity of the interaction with the desired molecule or species. Following this idea, many authors have reported different synthetic routes to obtain MNPs coated with a silica layer, which have been successful in inorganic ions and different DNA molecules or proteins separation [11, 14-16]. Ordered mesoporous silicas (OMS) appear as interesting materials in order to cover the MNPs because this kind of solids, such as MCM-41, consist of amorphous SiO_2 walls with a characteristic and well defined mesoporous arrangement, uniform pore size and high S_g which can achieve 1000 $m^2.g^{-1}$ [17]. Yang et al. [18] synthesized MNPs of magnetite (300 nm of diameter) which were first coated with a thin layer of amorphous silica and then with a layer of OMS, reaching a total coverage thickness of approximately 30 nm. The OMS coverage gives to the composite suitable properties (S_g of 378 $m^2.g^{-1}$) for its potential use in controlled drug release [18]. Finally, another advantage of using OMS is the absence of diffusional impediments inside the network pores [19].

The most widely magnetic iron phase studied and used to give magnetic properties to composites has been the magnetite (Fe_3O_4) [11, 14-16, 18, 20, 21]. However, the presence of Fe^{2+} ions in the magnetite structure, transforms this kind of composites as a

potential material with capability to catalyze the Fenton reaction, producing reactive oxygen species (ROS). Excessive ROS quantities in intracellular environment are associated with cytotoxic mechanisms such as protein oxidation, DNA damage, and oxidative stress [22]. Therefore, materials with magnetite in its structure would be incompatible with aqueous media involving biological systems or living species [23-25]. Taking in to account that maghemite (γ-Fe_2O_3) and magnetite have similar magnetic properties (bulk maghemite has an average saturation magnetization close to 74 $A.m^2.kg^{-1}$ while magnetite has 84 $A.m^{2.}kg^{-1}$ at room temperature [26]) development of magnetic composites based on maghemite, becomes an interesting alternative route because this phase has not Fe^{2+} ions in their structure.

The aim of the present work is to report a simple synthesis of a MCM-41structure grown up around pre-synthesized maghemite nanoparticles and to study the possible magnetic and structural changes in the maghemite NPs produced during its coverage with the mesoporous silica structure. The MCM-41 presence would produce the following advantages: a) avoids the MNPs degradation, increasing composite durability and stability, b) generates a composite with high values of specific surface area and a pores network without diffusional restrictions, c) provides silanols groups, which can be easily functionalized with a variety of organics functions.

2. Experimental

2.1 Materials

The syntheses were carried out using commercially available reagents. Diphenyl ether (99%), oleic acid (90%), oleylamine (>70%), iron(III) acetylacetonate (Fe(acac)$_3$) (97%) and tetraethyl ortosilicate (TEOS) were purchased from Aldrich Chemical Co., dibenzyl ether (98%) and ammonium hydroxide from Fluka and hexadecyl trimethyl

4

ammonium bromide (CTMABr) from ICN Biomedicals Inc. These reactants and ethanol and hexane, were used as they were received.

2.2 Synthesis of iron oxide nanoparticles.

Iron oxide nanoparticles were synthesized following the procedure described by Perez De Berti et al [27]. Briefly, a mixture of Fe(acac)$_3$ (4 mmol), oleic acid (12 mmol), oleyl amine (12 mmol) and diphenyl ether (40mL, boiling point= 261 ºC) was heated under magnetic stirring up to 200 ºC and maintained at this temperature for 45 minutes. Then the mixture was heated under reflux up to 265 ºC and was maintained at this temperature for another 45 min. The mixture was cooled at room temperature (RT) and 80 ml of ethanol were added, appearing a black precipitate. The solid was recovered by centrifugation. After that, the solid was dispersed in n-hexane in presence of oleic acid and oleylamine. Then, the non-dissolved impurities were isolated by centrifugation during 10 minutes at 6000 rpm. Finally, the nanoparticles were precipitated with ethanol. The MNPs were recovered by centrifugation (6000 rpm, 10 min) and then re-dispersed in n-hexane. The sample was called γ-Fe$_2$O$_3$.

2.3 Synthesis of composite iron oxide nanoparticles@MCM-41

The composite of iron oxide nanoparticles immersed in MCM-41 was performed via the alkaline hydrolysis of TEOS using CTMABr as directing agent of the mesoporous structure. Thus, 2.5 ml of γ-Fe$_2$O$_3$ suspension were added under magnetic stirring to a mixture composed by NH$_4$OH (102 ml), distilled water (135 ml) and CTMABr (1.0 g) at 40 ºC. Then, 5.0 ml of TEOS were added to this mixture stirring at 40 ºC during 120 min. The solid thus obtained, called γ-Fe$_2$O$_3$@MCM-41, was filtrated, washed with distilled water and dried at RT overnight. In order to remove the template agent, the sample γ-Fe$_2$O$_3$@MCM-41 was calcined in N$_2$ flow (150 cm^3.min^{-1}) following this

program: from RT to 510 ºC at 8 ºC.min^{-1}, after 1 hour at 510 ºC the N_2 flow was

changed by air flow (150 cm^3.min^{-1}) keeping this temperature during 6 hours. The

sample obtained was called γ-Fe_2O_3@MCM-41-C.

2.4 Samples Characterization

The samples were characterized by nitrogen adsorption at -196 ºC (BET), infrared

spectroscopy (FT-IR), uv-visible spectroscopy (UV-vis), X-ray diffraction (XRD) at

low angles, magnetic measurements (SQUID), Mössbauer spectroscopy at 25 and -260 º

C and transmission electron microscopy (TEM).

The textural properties, specific surface area (S_g), specific pore volume (V_p) and

pore diameter (D_p), were measured in a Micromeritics equipment ASAP 2020 V1.02 E.

Pore diameter distribution was determined using the Barret, Joyner and Halenda (BJH)

method.

Infrared spectra of dried samples mixed with KBr (1:100) were obtained on a Jasco

FT/IR-4200 spectrometer equipped with a Pike Diffuse IR cell with a resolution of 1

cm^{-1}. Two hundred to four hundred scans were accumulated in each case.

In order to determine the iron content, the sample was dissolved with HF. The Fe^{3+}

ions of this solution were reduced with hydroquinone and o-phenanthroline was used as

complexing agent. The iron content was determined by UV-visible spectroscopy in a

Perkin Elmer Lambda 35 UV/VIS Spectrometer equipment. All assays were made by

triplicate.

X-ray diffraction patterns at low angles were recorded on a Philips PW 1710 with

graphite monochromator Cu K$_\alpha$ (λ=1.54056 Å) radiation in the range 2θ=1.5-8° with

steps of 0.02° and counting time of 2 s/step.

The magnetic measurements were carried out using a Multipurpose Physical

Magnetic System (MPMS) superconducting quantum interference device (SQUID) from

6

Quantum Design. The magnetizations versus magnetic field (M-H) curves were recorded at -267 and 27 ºC up to a maximum magnetic field of 3980 kA.m^{-1}. Thermal dependences of the magnetization under zero field (ZFC) and field cooling (FC) conditions were recorded using an external field of 3.98 kA.m^{-1}. Combining the iron loading of the composite with the mass used in each measurement, all magnetic results can be normalized

The Mössbauer spectra were obtained in transmission geometry with a 512-channel constant acceleration spectrometer. A source of ^{57}Co in Rh matrix of nominally 50 mCi was used. Velocity calibration was performed against a 12 μm-thick α-Fe foil. All isomer shifts (δ) mentioned in this paper are referred to this standard. The temperature was varied between -260 and 27 ºC using an ARS Closed Cycle Cryocooler Model ARS 8200. The Mössbauer spectra were evaluated using the Recoil Spectral Analysis software [28]. Although some spectra display magnetic relaxation, for simplicity, Lorentzian lines with equal widths were considered for each component. The spectra were folded to minimize geometric effects.

Transmission electron microscopy (TEM) images were recorded on a Philips CM 200 UT microscope equipped with an ultra-twin objective lens and with a LaB6 filament (operated at 200 keV). The microscope was equipped with a CCD camera for digital acquisition; contrast and illumination were adjusted linearly using commercially available image treatment programs.

3.Results and discussion

To identify the iron species of the pre-synthesized MNPs, the Mössbauer spectra at temperatures -260, -243 and 25 ºC were obtained (Figure 1). The spectrum recorded at -260 ºC shows six lines with their inner sides slightly broadened and a central non-resolved signal. This spectrum was fitted with two sextuplets and one doublet. The corresponding hyperfine parameters are shown in Table 1. One of the sextuplets is

magnetically blocked and the other one is relaxing. The hyperfine parameters of both sextuplets can be attributed to Fe^{3+} ions located in tetrahedral (A) and octahedral (B) sites of γ-Fe_2O_3 [29]. However, small particle size effects inhibit to distinguish between both sites. We observe that the hyperfine magnetic fields are reduced in comparison with those corresponding to the bulk compound [29]. This could be due to the collective magnetic excitation phenomenon observed in very small particles below the blocking temperature [30] as well as to the relaxing effect.

The temperature at which the superparamagnetic relaxation time is equal to the timescale of the experimental technique is called the blocking temperature, T_B. At this temperature 50% of the Mössbauer signal is magnetically blocked. As it can be seen, in this sample T_B is smaller than -260 ºC.

On the other side, the doublet at -260 ºC could be assigned to Fe^{3+} surface ions complexed with oleic acid through carboxylate heads with bidentate coordination as it was demonstrated by FT-IR in our previous work [27]. At -243 ºC the relaxing fraction is more significant than the observed at -260 ºC. Finally, at 25 ºC, almost the entire population of the MNPs has collapsed into a central signal assigned to a relaxing sextuplet corresponding to particle fractions whose relaxation times become comparable to the Mössbauer characteristic time. Besides, there is a central doublet that can be assigned to a superparamagnetic γ-Fe_2O_3 and to a less extent to superficial Fe^{3+} ions complexed with oleic acid.

Figure 2 shows the FT-IR spectra of the composites γ-Fe_2O_3@MCM-41 and γ-Fe_2O_3@MCM-41-C. The presence of the surfactant (BrCTMA) is detected in the composite without calcination. Indeed, the two strong bands, at 2924 and 2852 cm^{-1}, are due to the anti-symmetric and symmetric stretching vibrations of –CH_2– groups of the carbon chains, respectively [31, 32]. The absorption band occurring at 1478 cm^{-1} arises from the –CH_2– bending or scissor mode of the surfactant tail. The remaining bands are

8

typical of the MCM-41 material. For example, the peak at 960 cm^{-1} can be assigned to the stretching of Si-OH, and the peak at 1100 cm^{-1} to the stretching Si-O-Si. Moreover, both the peak at 1630 cm^{-1} and the broad band between 3000-3700 cm^{-1} correspond to physisorbed water molecules [33].

The characteristics bands of oleic acid with bidentate coordination with surface Fe^{3+} of the MNPs are not detected. Feasibility, the strong alkaline medium of the synthesis gel produces the releasing of the oleate from the surface of the MNPs. As it will be discussed bellow, the absence of the coverage probably allows strong magnetic interactions between the MNPs. The action of these interactions could produce an approximation and/or agglomeration of the particles. Finally, in the calcined composite spectrum the characteristics bands of the BrCTMA have disappeared remaining only the typical MCM-41 bands (Figure 2).

The Mössbauer spectra of γ-Fe$_2$O$_3$@MCM-41 were obtained at -260 and 25 ºC (Figure 3 and Table 2). The spectrum recorded at -260 ºC shows six narrow resolved lines and a central non-resolved signal. This spectrum was fitted to two sextuplets with hyperfine field distributions and one singlet. The hyperfine parameters of both sextuplets can be attributed to Fe^{3+} ions located in tetrahedral (A) and octahedral (B) sites of magnetically blocked γ-Fe$_2$O$_3$ MNPs [29]. This result demonstrates that the MCM-41 synthesis process did not affect the iron oxide species. Besides, the blocking temperature is larger than that corresponding to the pre-synthesized MNPs (Tables 1 and 2). This result leads to deduce that the original MNPs could have undergone an agglomeration process, as it was previously described. The arising of the central singlet that replaces the doublet assigned to surface iron oleate in MNPs is coherent with this description. In the strong alkaline medium oleate anions could be replaced by OH$^-$ ions. In this way, the environment of the superficial Fe^{3+} ions would be very similar to the tetrahedral and octahedral sites of the inner γ-Fe$_2$O$_3$. Therefore, as these sites have a

9

high symmetry, they give rise to a singlet signal. Finally, at 25 ºC, almost the entire iron population has collapsed into a central signal that we fitted to a relaxing sextuplet that represents to those particles whose relaxing times are near the window experimental time.

The Mössbauer spectra of γ-Fe$_2$O$_3$@MCM-41-C were obtained at 25 and -260 ºC (Figure 4 and Table 3). The spectra at both temperatures are rather similar to those recorded for γ-Fe$_2$O$_3$@MCM-41 although a doublet instead of a singlet appears at 25 ºC. From this, we deduce that the iron oxide species have not changed after the calcination. This is a striking result since it is well known that when γ-Fe$_2$O$_3$ is heated in air at temperatures higher than 330-350 ºC, it transforms to the most stable thermodynamic compound, i. e., hematite (α-Fe$_2$O$_3$). In our case, possibly the coating effect of the MCM-41 on the MNPs inhibits the structural transformation. Therefore, as the composite preserves the ferrimagnetic response, it can be suitable for potential applications in the field of magnetic adsorbents. On the other hand, the doublet at 25 ºC could be assigned to Fe^{3+} paramagnetic ions diffused inside the MCM-41 walls located in highly distorted sites (Table 3), since a high quadrupole splitting value was obtained. The presence of this paramagnetic species will be confirmed by the magnetic results.

To magnetically characterize the samples and determine qualitatively the existence of magnetic interactions between the MNPs in γ-Fe$_2$O$_3$@MCM-41 we carried out M vs H and ZFC/FC magnetization measurements. Previously, we will analyse the results obtained on pre-synthesized MNPs. Figure 5a shows the M vs H loops taken at 25 and -267 ºC. All data have been normalized per gram of iron oxide mass. The M vs H loop at 25 ºC does not show hysteresis. This reversible behaviour observed in MNPs is typical of particles relaxing superparamanetically. The loop taken at -267 ºC shows hysteresis with a coercive field Hc= 7.16 kA.m^{-1}. The saturation magnetization normalized by the mass of Fe$_2$O$_3$ is about 44 A.m^2.kg^{-1}. This reduced Ms value in comparison with bulk

10

maghemite is usually found in very small maghemite particles and it is attributed to the surface spin disorder [34].

Figure 5b shows the ZFC and FC curves of the pre-synthesized MNPs. The ZFC curve shows a rather sharp maximum at about -258 ºC, which represents the blocking temperature T_B. Taking into account that T_B depends on the timescale of the experimental technique, a difference with the Mössbauer result would be expected. Well-above T_B, the ZFC and FC curves overlap due to at these temperatures the magnetization vector relaxes superparamagnetically. We observe that the FC curve increases monotonically as the temperature decreases along all the temperature range. Particularly, the continuous increment below T_B indicates that the magnetic interactions between MNPs are negligible and then the single-domains align along a weak magnetic field. Therefore, this result indicates that the oleate coverage not only prevents the action of exchange interactions between MNPs, but the interparticle distances of about 2-3 nm that establishes also neglects the magnetic dipolar interactions [29].

Figure 6a shows the M-H curves of γ-Fe$_2$O$_3$@MCM-41. The loop remains closed at 25 ºC, while at -267 ºC shows an hysteresis with a coercive field H_C= 27 kA.m^{-1}. Strikingly, the saturation magnetization decreases (Ms= 34 A.m^2.kg^{-1}) with respect to the Ms value of pre-synthesized MNPs. But the main difference arises from the ZFC and FC magnetization curves (Figure 6b). Indeed, the ZFC curve has a broad maximum at about T_B = -173 ºC and the FC curve flattens below T_B. The shift of T_B towards higher values, the broadening of the ZFC curve as well as the FC features, all indicate the existence of strong magnetic interactions between the MNPs when forming part of the composite [35]. This fact is consistent with the disappearance of the acid oleic coating observed by FT-IR that probably contributes to both the direct contact between MNPs and a reduction of the interparticle distances. The former facilitates the action of

exchange interactions between particles, while the later causes that the dipolar interactions between particles become considerable [36].

The magnetic results corresponding to γ-Fe_2O_3@MCM-41-C are displayed in Figures 7a and 7b. The M-H loop at -267 ºC shows the MNPs ferrimagnetic contribution plus a paramagnetic response. The presence of a paramagnetic phase is coherent with that found by Mössbauer spectroscopy, i.e., the calcination step produces the diffusion of a fraction of Fe^{3+} ions inside the MCM-41 matrix that behave as a paramagnet. After discounting the paramagnetic contribution, the saturation magnetization value for the MNPs of the calcined composite is 78 $A.m^2.kg^{-1}$, which is close to the Ms value of bulk γ-Fe_2O_3, while H_C= 15.9 $kA.m^{-1}$. We observe that the ZFC-FC curve shapes are similar to those recorded for γ-Fe_2O_3@MCM-41 but present a larger magnetization and the blocking temperature is T_B= -193 ºC. Therefore, the γ-Fe_2O_3@MCM-41-C results show that the interacting MNPs that form γ-Fe_2O_3@MCM-41 have experienced a sintering process after the surfactant was eliminated.

Figures 8a and 8b display TEM image of pre-synthesized γ-Fe_2O_3 MNPs and the size distribution obtained and fitted with a log-normal function respectively. The statistics parameters are shown in Table 4. The average size of the MNPs is about 3 nm, and no agglomeration is observed. The small difference between the arithmetic and geometric mean indicates that the distribution has a little skewness.

Figures 9a shows the micrograph of γ-Fe_2O_3@MCM-41-C and Figure 9b the size distribution of the MNPs. Here, we distinguish the ordered structure typical of MCM-41 with MNPs of maghemite "immersed" in the mesoporous solid. The average size of the MNPs in γ-Fe_2O_3@MCM-41-C is approximately three times larger than the diameter of the original of the pre-synthesized MNPs. This result confirms the sintering process describe above. Further, from the HRTEM micrograph (Figure 10) there is only one orientation of the crystalline planes of one of the MNPs located outside of the MCM-41

matrix. Therefore, the sintering process has produced a magnetic monodomain of about

9 nm, in agreement with the increase of the saturation magnetization observed in the M

vs H graph (Figure 6a). Besides, there is an amorphous silica shell which covers the

surface of this nanoparticle. This thin coating would be responsible of the thermal

stability of the nanoparticles located outside the mesoporous matrix.

The γ-Fe$_2$O$_3$@MCM-41 and γ-Fe$_2$O$_3$@MCM-41-C XRD patterns are displayed in

Figure 11. Both exhibit low-angle (100), (110) and (200) reflections confirming the

MCM-41 structure observed by TEM. The similar peak-widths and intensities show that

the calcination treatment did not affect the ordered structure. However, there is a

slightly shift towards higher angles of the three peaks compared with the non calcined

sample ones. This behavior can be assigned to a small contraction as a consequence of

the surfactant removal [37].

In order to obtain the textural properties of the γ-Fe$_2$O$_3$@MCM-41-C, N$_2$ adsorption-

desorption measurements at -196 ºC were made. The isotherm obtained is of type IV

(Fig. 12), characteristic of mesoporous materials such as MCM-41. The specific surface

area value of 494 m^2.g^{-1} is significantly higher than that reported in literature [14, 18].

The pore size distribution curve (Fig. 12 inset) is narrow with an average diameter of

2.6 nm, confirming the existence of a monomodal distribution belonging to the

mesoporous materials range. It is well established that a narrow pore size distribution

has important advantages for materials used in adsorptiont and/or separation

technologies, because diffusive processes are more homogeneous leading to a better

adsorption control. [19, 38]

In order to evaluate the potential application of the composite as adsorbent, we use

the methodology described in a previous work [38] to incorporate amino groups onto

the pores surface. After that, the magnetic composite material was tested for the

adsorption for chromium (VI) or copper (II) from water solutions. Experimental details

13

can be found in [38]. Briefly, batch-like experiments with a solid to metal solution ratio of 1 g.ml^{-1} were carried out for 24 h to ensure equilibrium conditions, with initial concentration of 130 ppm for the selected ion and constant stirring at 25 ºC. The maximum adsorption capacities were 43.5 and 31.6 mg.g^{-1} for Cr(VI) and Cu(II), respectively. After this experiment the composite was easily recovered from aqueous matrix using an external magnet, this is an important property for the separation of the adsorbent from aqueous medium and its re-utilization.

4. Conclusions

In this work we report a simple method to obtain a mesoporous MCM-41 structure grown up around pre-synthesized maghemite nanoparticles. The synthesis only requires to mix maghemite nanoparticles with the synthesis gel of MCM-41 and calcination in air. In spite of the presence in the synthesis gel of monodisperse 3 nm magnetic nanoparticles, the MCM-41 arrangement was obtained. The presence of mesoporous ordered silica structure produces a composite with a high specific surface area in comparison with previous results obtained by other authors using amorphous silica.

An unusual characteristic of this system is that the calcination treatment did not produce the expected phase transformation of maghemite to hematite. This indicates that the mesoporous structure acts as a protective layer of the magnetic phase. On the other hand, due to the basic environment in the MCM-41 synthesis gel, a sintering of the original nanoparticles occurred. This sintering leads to get a magnetization saturation value similar to that of the bulk maghemite compound. This is a very important result in order carry out an easy separation from an aqueous media and to recover the material with an external magnet after their use in an adsorption and/or separation processes. Due to its optimal features and the performance demonstrated on preliminary adsorption studies of Cr(VI) and Cu(II), this composite could have potential

applications in different important fields such as pollutants adsorption from aqueous matrix, biomolecules separation, drug delivery, etc.

References

[1] J. Hu, G. Chen, I.M.C. Lo, Removal and Recovery of Cr (VI) from Electroplating Wastewater by Maghemite Nanoparticles, Water Res. 39 (2005) 4528–4536. DOI: 10.1016/j.watres.2005.05.051.

[2] J.T. Mayo, C. Yavuz, S. Yean, L. Cong, H. Shipley, W. Yu, J. Falkner, A. Kan, M. Tomson, V.L. Colvin, The Effect of Nanocrystalline Magnetite Size on Arsenic Removal, Sci. Technol. Adv. Mater. 8 (2007) 71–75. DOI:10.1016/j.stam.2006.10.005.

[3] Ling Xu, Chen Guo, Feng Wang, Sen Zheng, Chun-Zhao Liu, A simple and rapid harvesting method for microalgae by in situ magnetic separation, Bioresour. Technol. 102 (2011) 10047–10051. DOI:10.1016/j.biortech.2011.08.021

[4] J. Rivas, M. Bañobre-López, Y. Piñeiro-Redondo, B. Rivas, M.A. López-Quintela, Magnetic Nanoparticles for Application in Cancer Therapy, J. Magn. Magn. Mater. 324, 21 (2012) 3499–3502. DOI: 10.1016/j.jmmm.2012.02.075.

[5] S.K. Sahu, A. Chakrabarty, D. Bhattacharya, S.K. Ghosh, P. Pramanik, Single Step Surface Modification of Highly Stable Magnetic Nanoparticles for Purification of His-tag Proteins, J. Nanopart. Res. 13 (2011) 2475–2484. DOI: 10.1007/s11051-010-0140-y.

[6] Y. Sui, Y. Cui, Y. Nie, G-M. Xia, G-X. Sun, J-T. Han, Surface Modification of Magnetite Nanoparticles Using Gluconic Acid and Their Application in Immobilized Lipase, Coll. Surf., B. 93 (2012) 24–28. DOI: 10.1016/j.colsurfb.2011.11.054.

[7] G.F. Goya, V. Grazú, M.R. Ibarra, Magnetic Nanoparticles for Cancer Therapy. Curr. Nanosci. 4 (2008) 1-16. DOI: 10.2174/157341308783591861.

[8] S.T. Selvan, T.T.Y. Tan, D.K. Yi, N.R Jana, Functional and Multifunctional Nanoparticles for Bioimaging and Biosensing, Langmuir 26 (2010) 11631–11641. DOI: 10.1021/la903512m.

[9] V.L. Lassalle, R.D. Zysler, M.L. Ferreira, Novel and Facile Synthesis of Magnetic Composites by a Modified Co-precipitation Method, Mater. Chem. Phys.130 (2011) 624– 634. DOI: Mater. Chem. Phys. 2011, 130, 624– 634.

[10] H-B. Xia, J. Yi, P-S. Foo, B. Liu, Facile Fabrication of Water-Soluble Magnetic Nanoparticles and Their Spherical Aggregates, Chem. Mater. 19 (2007) 4087-4091. DOI: 10.1021/cm070918q.

[11] I.J. Bruce, J. Taylor, M. Todd, M.J. Davies, E. Borioni, C Sangregorio, T. Sen, Synthesis, Characterisation and Application of Silica-magnetite Nanocomposites, J. Magn. Magn. Mater. 284 (2004) 145–160. DOI: 10.1016/j.jmmm.2004.06.032.

[12] S. Kralj, D. Makovec, S. Campelj, M. Drofenik, Producing Ultra-thin Silica Coatings on Iron-Oxide Nanoparticles to Improve their Surface Reactivity, J. Magn. Magn. Mater. 322 (2010) 1847–1853. DOI: 10.1016/j.jmmm.2009.12.038.

[13] Y. Li, J.S. Church, A.L. Woodhead, Infrared and Raman Spectroscopic Studies on Iron Oxide Magnetic Nano-Particles and their Surface Modifications, J. Magn. Magn. Mater. 324 (2012) 1543–1550. DOI: 10.1016/j.jmmm.2011.11.065.

[14] J. Wang, S. Zheng, Y. Shao, J. Liu, Z. Xu, D. Zhu, Amino-Functionalized $Fe_3O_4@SiO_2$ Core-Shell Magnetic Nanomaterial as a Novel Adsorbent for Aqueous

Heavy Metals Removal, J. Colloid. Interface Sci. 349 (2010) 293-299. DOI: 10.1016/j.jcis.2010.05.010.

[15] C. Chiang, C. Sung, C. Chen, Application of Silica–Magnetite Nanocomposites to the Isolation of Ultrapure Plasmid DNA from Bacterial Cells, J. Magn. Magn. Mater. 305 (2006) 483–490. DOI: 10.1016/j.jmmm.2006.02.088.

[16] P.I. Girginova, A.L. Daniel-da-Silva, C.B. Lopes, P. Figueira, M. Otero, V.S. Amaral, E. Pereira, T. Trindade, Silica Coated Magnetite Particles for Magnetic Removal of Hg^{2+} from Water, J. Colloid. Interface Sci. 345 (2010) 234–240. DOI: 10.1016/j.jcis.2010.01.087.

[17] Q. Cai, W. Lin, F. Xiao, W. Pang, X. Chen, B. Zou, The Preparation of Highly Ordered MCM-41 with Extremely Low Surfactant Concentration, Microporous Mesoporous Mater. 32 (1999) 1–15. DOI: 10.1016/S1387-1811(99)00082-7.

[18] P. Yang, Z. Quan, Z. Hou, C. Li, X. Kang, Z. Cheng, J. Lin, A Magnetic, Luminescent and Mesoporous Core–Shell Structured Composite Material as Drug Carrier, Biomater. 30 (2009) 4786–4795. DOI: 10.1016/j.biomaterials.2009.05.038.

[19] L. Mercier, T. Pinnavaia, Heavy Metal Ion Adsorbents Formed by the Grafting of a Thiol Functionality to Mesoporous Silica Molecular Sieves: Factors Affecting Hg(II) Uptake, Environ. Sci. Technol. 32 (1998) 2749-2754. DOI: 10.1021/es970622t.

[20] H. Setyawan, F. Fajaroh, W. Widiyastuti, S. Winardi, I.W. Lenggoro, N. Mufti, One-Step Synthesis of Silica-Coated Magnetite Nanoparticles by Electrooxidation of Iron in Sodium Silicate Solution, J. Nanopart. Res. 14 (2012) 807-813. DOI: 10.1007/s11051-012-0807-7.

[21] Z. Surowiec, J. Goworek, J. Ryczkowski, M. Budzyński, M. Wiertel, J. Sarzyński, Mössbauer study of magnetite nanowire in MCM-41 type mesoporous silica templates, Nukleonika 52 (2007) (Supplement 1) S33−S36

[22] M. C. R. Symons, J.M.C. Gutteridge, Free Radicals and Iron: Chemistry, Biology, and Medicine; Oxford University Press: Oxford, U.K. 1998.

[23] M. Auffan, J. Rose, J-Y. Bottero, G.V. Lowry, J-P Jolivet, M.R. Wiesner, Towards a Definition of Inorganic Nanoparticles from an Environmental, Health and Hafety Perspective, Nat. Nanotechnol. 4 (2009) 634–641. DOI: 10.1038/nnano.2009.242.

[24] A.K. Gupta, A.S. Curtis, Surface Modified Superparamagnetic Nanoparticles for Drug Delivery: Interaction Studies with Human Fibroblasts in Culture, J. Mater. Sci.: Mater. Med. 15 (2004) 493-496. DOI: 10.1023/B:JMSM.0000021126.32934.20.

[25] N. Singh, J.S. Jenkins, R. Asadi, S.H. Doak, Potential Toxicity of Superparamagnetic Iron Oxide Nanoparticles (SPION), Nano Rev. 1 (2010) 5358-5372. DOI: 10.3402/nano.v1i0.5358.

[26] C.J. Goss, Saturation Magnetisation, Coercivity and Lattice Parameter Changes in the System Fe_3O_4-γFe_2O_3, and their Relationship to Structure, Phys. Chem. Miner. 16 (1988) 164-171. DOI: 10.1007/BF00203200.

[27] I.O. Perez De Berti, M.V. Cagnoli, G. Pecchi, J.L. Alessandrini, S.J. Stewart, J.B. Bengoa, S.G. Marchetti, Alternative Low-Cost Approach to the Synthesis of Magnetic Iron Oxide Nanoparticles by Thermal Decomposition of Organic Precursors, Nanotechnol. 24 (2013) 175601-175611. DOI: 10.1088/0957-4484/24/17/175601.

[28] V. Lagarec, D.G. Rancourt, Mossbauer Spectral Analysis Software Dep. of Phys. University of Otawa, Version 1.0. 1998.

[29] E. Murad, Clays and Clay Minerals: What can Mössbauer Spectroscopy do to Help Understand Them?, Hyperfine Interact. 17 (1998) 39–70. DOI: 10.1023/A:1012635124874.

[30] S. Mørup H. Topsøe, Mössbauer Studies of Thermal Excitations in Magnetically Ordered Microcrystals, Appl. Phys.   11 (1976) 63–66. DOI: 10.1007/BF00895017.

[31] R.P. Sperline, Y. Song, H. Freiser, Fourier Transform Infrared Attenuated Total Reflection Spectroscopy Linear Dichroism Study of Sodium Dodecyl Sulfate Adsorption at the Al_2O_3/Water Interface Using Al_2O_3-Coated Optics, Langmuir 8 (1992) 2183-2191. DOI: 10.1021/la00045a019

[32] A.R. Hind, S.K. Bhargava, S.C. Grocott, Attenuated Total Reflection Fourier Transform Infrared Spectroscopic Investigation of the Solid/Aqueous Interface of Low Surface Area, Water-Soluble Solids in High Ionic Strength, Highly Alkaline, Aqueous Media, Langmuir 13 (1997) 3483-3487. DOI: 10.1021/la970141n.

[33] K.C. Souza, G. Salazar-Alvarez, J.D. Ardisson, W.A.A. Macedo, E.M.B. Sousa, Mesoporous Silica–Magnetite Nanocomposite Synthesized by Using a Neutral Surfactant, Nanotechnol. 19 (2008) 185603-185609. DOI:10.1088/0957-4484/19/18/185603.

[34] J. M. D. Coey, Noncollinear Spin Arrangement in Ultrafine Ferrimagnetic Crystallites, Phys. Rev. Lett. 27, 17 (1971) 1140-1142. DOI: 10.1103/PhysRevLett.27.1140.

[35] S. Mørup, M.F. Hansen, C. Frandsen, Magnetic interactions between nanoparticles, J. Nanotechnol. 1 (2010) 182–190. DOI:10.3762/bjnano.1.22.

[36] D. Fiorani, J.L. Dormann, R. Cherkaoui, E. Tronc, F. Lucari, F. D'Orazio, L. Spinu, M. Nogues, A. Garcia, A.M. Testa, Collective Magnetic State in Nanoparticles Systems, J. Magn. Magn. Mater. 196-197 (1999) 143–147. DOI: 10.1016/S0304-8853(98)00694-5.

[37] S. Hitz, R. Prins, Influence of Template Extraction on Structure, Activity, and Stability of MCM-41 Catalysts, J. Catal. 168 (1997) 194–206. DOI: 10.1006/jcat.1997.1659.

[38] N. Fellenz, P. Martin, S. Marchetti, F. Bengoa, Aminopropyl-modified mesoporous silica nanospheres for the adsorption of Cr(VI) from water, J. Porous Mater. 22 (3) 2015 729-738. DOI: 10.1007/s10934-015-9946-4.

Figure Captions

Figure 1. Mössbauer spectra of MNPs at different temperatures.

Figure 2. FT-IR spectra of γ-Fe$_2$O$_3$@MCM-41 and γ-Fe$_2$O$_3$@MCM-41-C.

Figure 3. Mössbauer spectra of γ-Fe$_2$O$_3$@MCM-41 at different temperatures.

Figure 4. Mössbauer spectra of γ-Fe$_2$O$_3$@MCM-41-C at different temperatures

Figure 5. a. M versus H loops at 27 and -267 ºC for MNPs. **b.** ZFC–FC magnetization curves for MNPs.

Figures 6. a. M versus H loops at 27 and -267 ºC for γ-Fe$_2$O$_3$@MCM-41. **b.** ZFC–FC magnetization curves for γ-Fe$_2$O$_3$@MCM-41.

Figures 7. a. M versus H loops at 27 and -267 ºC for γ-Fe$_2$O$_3$@MCM-41-C. **b.** ZFC–FC magnetization curves for γ-Fe$_2$O$_3$@MCM-41-C.

Figure 8. a. TEM image of MNPs. **b.** Size distributions of MNPs from TEM measurements. Solid line was obtained fitting the results by assuming a log-normal distribution.

Figure 9. a. TEM image of γ-Fe$_2$O$_3$@MCM-41-C. **b.** Size distributions of γ-Fe$_2$O$_3$@MCM-41-C from TEM measurements. Solid line was obtained fitting the results by assuming a log-normal distribution.

Figure 10. HRTEM image of γ-Fe$_2$O$_3$@MCM-41-C

Figure 11. DRX of γ-Fe$_2$O$_3$@MCM-41 and γ-Fe$_2$O$_3$@MCM-41-C.

Figure 12. N_2 adsorption-desorption isotherm at -196 ºC of γ-Fe$_2$O$_3$@MCM-41-C,

inset: pore size distribution curve.

Table 1: Mössbauer parameters of MNPs at different temperatures.

Species	Parameters	25 ºC	-243 ºC	-260 ºC
γ-Fe$_2$O$_3$ (A+B sites)	H^a (kG)	-----	459 ± 7	468 ± 3
	δ^b (mm/s)	-----	0.45 ^{c}	0.46 ^{c}
	2ε^d (mm/s)	-----	0 ^{c}	0 ^{c}
	%	-----	13 ± 3	25 ± 4
Relaxing signal	H^a (kG)	300 ^{c}	403 ± 8	434 ± 8
	δ^b (mm/s)	0.34 ± 0.04	0.45 ^{c}	0.46 ^{c}
	2ε^d (mm/s)	0 ^{c}	0 ^{c}	0 ^{c}
	%	77 ± 7	85 ± 4	73 ± 6
superficial Fe^{3+} coordinated with oleic acid	Δ^e (mm/s)	0.69 ± 0.07	0.7 ^{c}	0.7 ^{c}
	δ^b (mm/s)	0.30 ± 0.03	0.27 ± 0.08	0.2 ± 0.1
	%	23 ± 5	2 ^{c}	2 ^{c}

^{a}: hyperfine magnetic field; ^{b}: isomer shift referred to α -Fe at 25 ºC; ^{c}:parameter held

fixed in fitting; ^{d}:2ε: quadrupole shift; ^{e}: quadrupole splitting.

21

Table 2: Mössbauer parameters of γ-Fe$_2$O$_3$@MCM-41 at different temperatures.

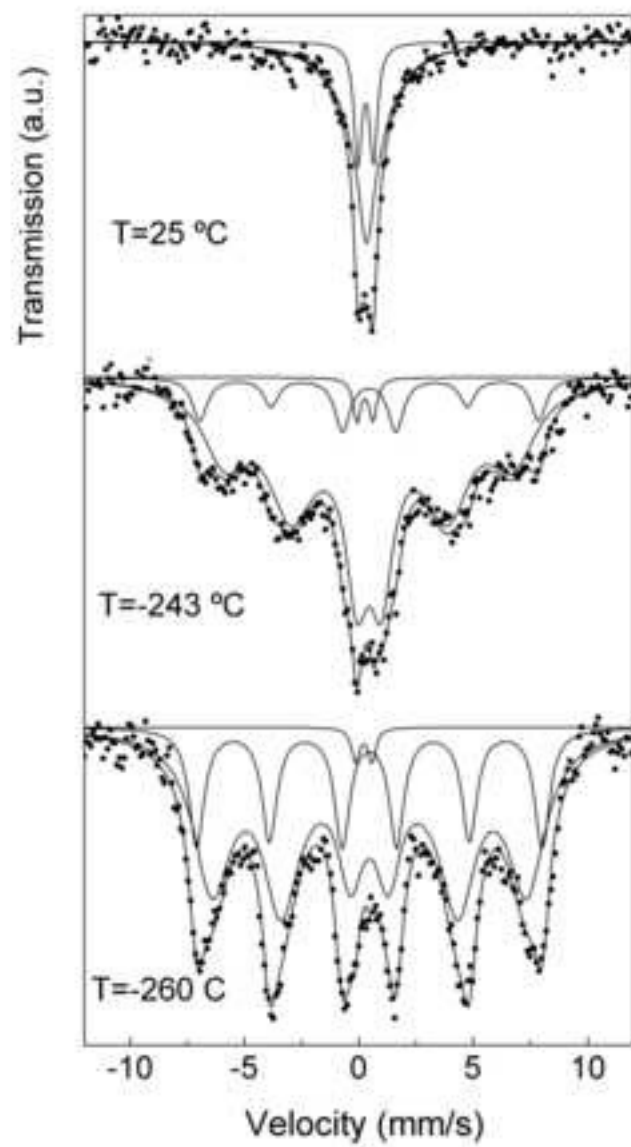| Species	Parameter	25 ºC	-260 ºC
	H^a (kG)	300 ^{b}	-----
Relaxing signal	δ^c (mm/s)	0.38 ± 0.04	-----
	2ε^d (mm/s)	0 ^{b}	-----
	%	96 ± 3	-----
	H^a (kG)	-----	495 ± 10
γ-Fe$_2$O$_3$ (A Sites)	δ^c (mm/s)	-----	0.40 ± 0.07
	2ε^d (mm/s)	-----	-0.2 ± 0.1
	%	-----	25 ± 6
	H^a (kG)	-----	517.3 ± 0.9
γ-Fe$_2$O$_3$ (B Sites)	δ^c (mm/s)	-----	0.45 ± 0.01
	2ε^d (mm/s)	-----	0.01 ± 0.02
	%	-----	73 ± 6
superficial Fe^{3+}	δ^c (mm/s)	0.28 ^{b}	0.3 ± 0.2
coordinated with OH$^-$	%	4 ^{b}	2 ± 1

^{a}: hyperfine magnetic field; ^{b}: parameter held fixed in fitting ; ^{c}: isomer shift (all the isomer shifts are referred to α -Fe at 25 ºC); ^{d}: quadrupole shift.
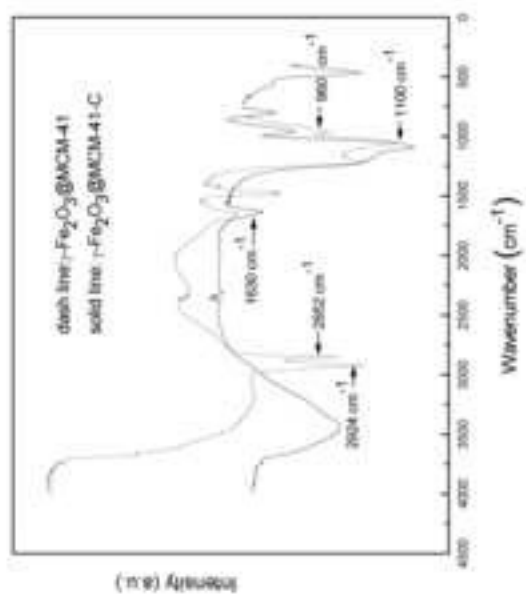
Table 3: Mössbauer parameters of γ-Fe$_2$O$_3$@MCM-41-C at different temperatures.

Species	Parameters	25 ºC	-260 ºC
Relaxing signal	H^a (kG)	300 ^{b}	-----
	δ^c (mm/s)	0.29 ± 0.03	-----
	2ε^d (mm/s)	0 ^{b}	-----
	%	89 ± 7	-----
γ-Fe$_2$O$_3$ (A Sites)	H^a (kG)	-----	484 ± 9
	δ^c (mm/s)	-----	0.40 ± 0.05
	2ε^d (mm/s)	-----	0.1 ± 0.1
	%	-----	43 ± 7
γ-Fe$_2$O$_3$ (B Sites)	H^a (kG)	-----	510 ± 2
	δ^c (mm/s)	-----	0.40 ± 0.05
	2ε^d (mm/s)	-----	0.03 ± 0.04
	%	-----	53 ± 7
Fe^{3+} diffused inside SiO$_2$ walls	Δ^e (mm/s)	0.9 ± 0.1	1.5 ± 0.3
	δ^c (mm/s)	0.35 ± 0.08	0.5 ± 0.1
	%	11 ± 4	4 ± 2

^{a}: hyperfine magnetic field; ^{b}: parameter held fixed in fitting; ^{c}: isomer shift (all the isomer shifts are referred to α -Fe at 25 ºC); ^{d}: quadrupole shift; ^{e}: quadrupole splitting.

Table 4: Statistics parameters of MNPs and γ-Fe₂O₃@MCM-41-C obtained by TEM.

TEM	$\mu_g{}^a$ (nm)	$\sigma_g{}^b$ (nm)	$\mu_a{}^c$ (nm)	Mode^d (nm)
MNPs	3.4	1.2	3.5	3.3
γ-Fe₂O₃@MCM-41-C	8.4	1.6	9.3	6.7

[a]: geometric mean; [b]: geometric variance; [c]: aritmetic mean.

Figure

Figure

Figure

Figure

0.02 µm

Figure

Figure

200 nm

Figure

Figure

Figure

Figure

Figure

Figure

Figure

Figure

Figure